A well-posed and effective high-order Impedance Boundary Condition for the time-harmonic scattering problem from a multilayer coated 3-D object

Bruno Stupfel, Pierre Payen, Olivier Lafitte

Progress In Electromagnetics Research B, Vol. 94, 127–144, 2021

A Well-Posed and Effective High-Order Impedance Boundary Condition for the Time-Harmonic Scattering Problem from a Multilayer Coated 3-D Object

Bruno Stupfel[1, *], Pierre Payen[1], and Olivier Lafitte[2]

Abstract—The time-harmonic scattering problem from an isotropic multilayer coated 3-D object is considered. The coating is modeled by an impedance boundary condition (IBC) prescribed on the outer surface of the coating. The standard Leontovich IBC is local and constitutes a poor approximation for low index materials. A possible remedy is to employ high order IBCs (HOIBCs) involving tangential differential operators multiplied by coefficients. A generic HOIBC formulation (termed here IBC3) with five coefficients is considered here. Sufficient uniqueness conditions (SUCs) are derived for the corresponding Maxwell's problem (i.e., Maxwell's equations in free-space, radiation condition at infinity and IBC3 on the surface). The IBC3 coefficients are obtained by minimizing, with the SUCs as constraints, the error between either the exact and IBC3 impedances (local planar approximation) or the exact and IBC3 Mie series coefficients (local spherical approximation). Finally, the IBC3 is numerically implemented in a well-posed EFIE+MFIE formulation. Numerical results obtained on 3D objects demonstrate the high accuracy achieved with the constrained IBC3.

1. INTRODUCTION

The full-wave solution of the time-harmonic scattering problem from an isotropic multilayer coated 3D object via a finite or boundary element method is computationally intensive when parametric studies (uncertainty analysis, optimization of the shape and/or coating of the object, etc.) are required. A well-known approximation consists in substituting to the coating an impedance boundary condition (IBC) prescribed on its closed outer surface Γ. This IBC, implemented in an integral equation, avoids the costly solution of Maxwell's equations inside the material layers. The simplest and most popular one, termed here IBC0, connects the tangential components of the electric and magnetic fields via a scalar [1]. It is strictly local (an exact IBC is non local) and constitutes a good approximation for high index materials only.

For a thin monolayer of thickness d, effective and well-posed high order IBCs (HOIBCs) of order k have been obtained via a multiscale asymptotic expansion of the exact solution with respect to d [2–4], and it has been mathematically and numerically demonstrated that, if Γ is smooth enough, the error between this expansion and the exact solution scales as $O(d^{k+1})$. Regarding a low index and not necessarily thin multilayer, essentially heuristic HOIBCs involving tangential derivatives of the tangent electric and magnetic fields on Γ are available in the literature [5–13]. A generalized IBC was first proposed in the space domain for 2-D problems [5] where the coefficients in the IBC are derived from the exact reflection coefficient calculated for a plane wave incident on a planar layer. It was extended later on to 3-D electromagnetic problems [6]. The analytical derivation of the coefficients in the IBC from

Received 28 July 2021, Accepted 17 October 2021, Scheduled 13 December 2021
* Corresponding author: Bruno Stupfel (bruno.stupfel@cea.fr).
[1] CEA, DAM, CESTA, F-33114 Le Barp, France. [2] LAGA, Université Paris 13, Villetaneuse, France and UMI3457 CRM, Université de Montréal, Montréal, Canada.

the exact reflection coefficient or the exact impedance necessitates ad-hoc complicated approximations that are difficult to apply to a multilayer coating [6, 8] and, to date, no numerical implementation of the GIBC for the solution of a general 3-D problem is known. In the spectral domain (infinite plane or 2D circular cylinder) an effective HOIBC with five coefficients has been proposed in [7] where the IBC coefficients are calculated in such a way as to yield an impedance as close as possible to the exact one (local planar or cylindrical approximation: LPA or LCA) in a large angular range including evanescent incident waves, and this HOIBC has been successfully applied to axisymmetric bodies [7]. A corresponding space domain formulation, termed here IBC3, has been proposed in [8] that can be applied to arbitrary 3D objects, and has been numerically implemented in MoM formulations [11–13].

The important issue of uniqueness of the solution of the Maxwell's problem (i.e., Maxwell's equations in free-space, radiation condition at infinity and HOIBC on Γ) is discussed in [9, 11] where sufficient uniqueness conditions (SUCs) are proposed for some HOIBCs. New SUCs specific to the IBC3 with five coefficients are presented here. Then the IBC3 is numerically implemented in the combined electric and magnetic field integral equations formulation (EFIE+MFIE) with the electric and magnetic currents as unknowns. This formulation has been employed in the past for the IBC0 [14, 15] and yields accurate results when the IBC0 is valid. The IBC3 involves the discretization of the surface divergence of $\underline{n}\times$ RWG functions. This problem has been circumvented in [16] for the IBC0 and in [12] for the IBC3 by using Buffa-Christianssen functions that, however, increase the computational cost. Instead, the computationally very cheap $div2curl$ and $curl2div$ transformations [10, 11, 17] are employed here, and the costly inversion of a full impedance matrix involved in the formulation proposed in [11] is suppressed.

This paper is organized as follows. The IBC3 is formulated in Section 2. Its coefficients are optimized for an infinite plane (LPA) or a sphere (local spherical approximation: LSA). Geometry independent SUCs are derived and the efficiency of the IBC3 constrained by these SUCs is evaluated first on an infinite plane illuminated by incident homogeneous or inhomogeneous (evanescent) plane waves, and then on a sphere. Section 3 is devoted to the IBC3 implementation in the well-posed EFIE+MFIE formulation and numerical results obtained on 3D objects are presented in Section 4. Conclusions are proposed in Section 5. Time dependence $\exp(i\omega t)$ is assumed and suppressed throughout.

2. WELL-POSED IBC3

The IBC3 is formulated in Section 2.1. Its coefficients are obtained in Section 2.2 and SUCs are derived in Section 2.3.

2.1. Formulation

We set

$$\begin{aligned} \underline{V}_t = -\underline{n}\times(\underline{n}\times\underline{V});\quad L_D\underline{V}_t = \underline{\nabla}_t\nabla_t\cdot\underline{V}_t;\quad L_R\underline{V}_t = \underline{curl}_\Gamma curl_\Gamma\underline{V}_t \\ curl_\Gamma\underline{V}_t = -\nabla_t\cdot(\underline{n}\times\underline{V}_t);\quad \underline{curl}_\Gamma u = -\underline{n}\times\underline{\nabla}_t u \end{aligned} \tag{1}$$

where subindex t indicates the tangential components of a vector or operator, u a scalar, and $\underline{n}$ the outward directed normal to Γ. From the identities in [24], we also have

$$L_R\underline{V}_t = \underline{curl}_t\{\underline{n}(\underline{n}\cdot\underline{curl}_t\underline{V}_t)\};\quad \underline{curl}_t\underline{V} = \underline{\nabla}\times\underline{V} - \underline{n}\times\partial_n\underline{V} \tag{2}$$

The IBC3 reads

$$\begin{aligned} L_E\underline{E}_t = L_J\underline{J} \\ L_E = 1 + b_1L_D - b_2L_R\ ;\ L_J = a_0 + a_1L_D - a_2L_R \end{aligned} \tag{3}$$

$\underline{E}$ is the electric field and $\underline{J} = \underline{n}\times\underline{H}$ where the magnetic field $\underline{H}$ stands for $\eta_0\underline{H}$ (η_0 is the free-space impedance). It is obtained from Eq. (22) in [8] by performing the cross product of this equation with $\underline{n}$ and using the identities

$$\underline{n}\times L_D(\underline{n}\times\underline{V}_t) = L_R\underline{V}_t;\quad \underline{n}\times L_R(\underline{n}\times\underline{V}_t) = L_D\underline{V}_t \tag{4}$$

easily derived from Eq. (1) and the identities in [24]. Depending on the values of the coefficients, the IBC3 yields the IBC0, exact when the plane is illuminated in normal incidence,

$$IBC0:\ \underline{E}_t = a_0\underline{J} \tag{5}$$

the IBC1 in [11] when $a_1 = a_2$, $b_1 = b_2$, and the IBC02 when $b_1 = b_2 = 0$.

2.2. Calculation of the Coefficients in (3)

First the IBC3 coefficients are computed as in [11] by invoking the LPA: at an arbitrary point on Γ, provided Γ is smooth enough, the curved coating is replaced by the infinite planar one with the same characteristics. Then we compute them on a sphere (LSA), thus taking into account two identical curvatures.

2.2.1. Planar Coating

We consider a planar N layers structure made up of homogeneous isotropic materials and backed by the IBC0 in Eq. (5) where $a_0 = Z_b$ is known, with $\mathrm{Re}(Z_b) \geq 0$; if $Z_b = 0$ the coating is backed by a perfect electric conductor (PEC). $z = 0$ is the outer surface of the coating (Γ is the (xOy) plane). $\underline{E}$ and $\underline{H}$ are y independent because the coating is translationally invariant along x and y. Their cartesian components are, for TM and TE polarizations and $z \geq 0$,

$$\begin{aligned} TM:\ \underline{H} = (0,H,0)^t\ ,\ \underline{E} = \frac{i}{k}(\partial_z H, 0, -\partial_x H)^t \\ \underline{J} = (-H,0,0)^t \\ TE:\ \underline{E} = (0,E,0)^t\ ,\ \underline{H} = -\frac{i}{k}(\partial_z E, 0, -\partial_x E)^t \\ \underline{J} = (0,H_x,0)^t \end{aligned} \tag{6}$$

$k = 2\pi/\lambda_0 = \omega/c$ is the free-space wave number (c is the light velocity). In TE polarization[†] we have

$$\begin{aligned} E &= e^{iksx}\left(e^{izk\xi_0} + r^{TE}e^{-izk\xi_0}\right);\quad \xi_0 = \sqrt{1-s^2} \\ H_x &= \xi_0 e^{iksx}\left(e^{izk\xi_0} - r^{TE}e^{-izk\xi_0}\right) \end{aligned} \tag{7}$$

The first r.h.s. term is the incident wave ($\underline{E}^{inc}, \underline{H}^{inc}$) and the second one the reflected (or scattered) wave ($\underline{E}^s, \underline{H}^s$). In Eq. (7) parameter s characterizes these waves: if $s \leq 1$ they are propagative (planar homogeneous) with $s = \sin\theta$ where θ is the real incidence angle counted from the z axis; if $s > 1$, they are evanescent (planar inhomogeneous) and $\mathrm{Im}(\xi_0) \leq 0$ to satisfy the boundary condition at infinity. The latter are considered because evanescent surface (or guided) waves may propagate inside the coating [18]. Reporting Eq. (3) into Eq. (7) with $\underline{E} = \underline{E}^{inc} + \underline{E}^s$, $\underline{H} = \underline{H}^{inc} + \underline{H}^s$ yields $r^{TE} = [a_0\xi_0 - 1 + s^2(b_2 - a_2\xi_0)]/[a_0\xi_0 + 1 - s^2(b_2 + a_2\xi_0)]$. Following along the same lines in TM and from the following standard definition of the impedances Z^{TM}, Z^{TE}

$$\underline{E}_t = \begin{pmatrix} Z^{TM} & 0 \\ 0 & Z^{TE} \end{pmatrix} \underline{J} \tag{8}$$

with

$$Z^{TM} = \frac{\xi_0\left(1 + r^{TM}\right)}{1 - r^{TM}};\quad Z^{TE} = \frac{1 + r^{TE}}{\xi_0\left(1 - r^{TE}\right)} \tag{9}$$

we get, as in [7],

$$Z^{TM} = Z^{TM}_{ibc} = \frac{a_0 - a_1k^2s^2}{1 - b_1k^2s^2};\quad Z^{TE} = Z^{TE}_{ibc} = \frac{a_0 - k^2a_2s^2}{1 - k^2b_2s^2} \tag{10}$$

where subindex *ibc* stands for the approximate impedance derived from the IBC3. The exact impedances $Z^p_{ex}(s)$ with $p = TM, TE$ are obtained from Eq. (9) where $r^p = r^p_{ex}$ computed from the multilayer as indicated in [19]. Then $\chi = (a_0, a_1, a_2, b_1, b_2)^t \in \mathbb{C}^5$ is obtained by minimizing the error between the exact and approximate impedances for $s \in [0, s_M]$ where s_M is a given maximum value of s

$$\chi^{LPA} = \mathrm{argmin}\left\{\sum_{p=TM,TE}\int_0^{s_M}\left|Z^p_{ex}(s) - Z^p_{ibc}(s,\chi)\right| ds\right\} \tag{11}$$

as indicated in [11] for the derivation of the IBC1 coefficients.

[†] TM is obtained from TE via the following operations: $\mu \to \epsilon$, $Z \to 1/Z$, $r^{TE} \to -r^{TM}$.

2.2.2. Spherical Coating

We consider a PEC sphere of radius R. d is the total thickness of the coating on the outermost boundary of which the IBC3 is prescribed. In spherical coordinates and for $r \geq R+d$ the scattered field is given by the following standard Mie series that read, with the same notations as in [20],

$$\begin{aligned}\underline{E}^s(\underline{r}) = -\sum_{n=1}^{\infty} f_n \left[\alpha_n \overline{\underline{M}}_{1n}(\underline{r}) + \beta_n \overline{\underline{N}}_{1n}(\underline{r})\right. \\ \left. +n(n+1)\left(\alpha_n \overline{\underline{M}}_{-1n}(\underline{r}) - \beta_n \overline{\underline{N}}_{-1n}(\underline{r})\right)\right] \\ \underline{H}^s(\underline{r}) = -i\sum_{n=1}^{\infty} f_n \left[\beta_n \overline{\underline{M}}_{1n}(\underline{r}) + \alpha_n \overline{\underline{N}}_{1n}(\underline{r})\right. \\ \left. -n(n+1)\left(\beta_n \overline{\underline{M}}_{-1n}(\underline{r}) - \alpha_n \overline{\underline{N}}_{-1n}(\underline{r})\right)\right]\end{aligned} \tag{12}$$

In what follows, α_n^{ex}, β_n^{ex} denote the coefficients that take the coating exactly into account and α_n^{ibc}, β_n^{ibc} the approximate ones derived by substituting the above expressions of $\underline{E}^s$, $\underline{H}^s$ in Eq. (3):

$$\begin{aligned}\alpha_n^{ibc}(\chi) &= \frac{\widetilde{j}_n(x)}{\widetilde{h}_n(x)}\left[\frac{i(a_0-\gamma_n a_2)+(1-\gamma_n b_2)/A_n}{i(a_0-\gamma_n a_2)+(1-\gamma_n b_2)/\overline{A}_n}\right] \\ \beta_n^{ibc}(\chi) &= \frac{j_n(x)}{h_n(x)}\left[\frac{i(a_0-\gamma_n a_1)-A_n(1-\gamma_n b_1)}{i(a_0-\gamma_n a_1)-\overline{A}_n(1-\gamma_n b_1)}\right] \\ x = k(R+d)\ \gamma_n &= \frac{n(n+1)}{x^2} \\ A_n = \frac{\widetilde{j}_n(x)}{x j_n(x)};\ \ \overline{A}_n &= \frac{\widetilde{h}_n(x)}{x h_n(x)}\end{aligned} \tag{13}$$

$j_n(\cdot)$, $h_n(\cdot)$ are the spherical Bessel and Hankel functions of order n and $\widetilde{j}_n(x) = \frac{d}{dx}(x j_n(x))$, $\widetilde{h}_n(x) = \frac{d}{dx}(x h_n(x))$. The IBC3 coefficients are obtained by minimizing the error between the approximate and exact coefficients for $n \leq N$ where the series in Eq. (12) are truncated at $n = N$:

$$\chi^{LSA} = \text{argmin}\left\{\sum_{n=1}^{N}\left|\alpha_n^{ex} - \alpha_n^{ibc}(\chi)\right| + \left|\beta_n^{ex} - \beta_n^{ibc}(\chi)\right|\right\} \tag{14}$$

2.3. Well-Posedness

It is well known [21] that the solution of the Maxwell's problem is unique if

$$\text{Re}\left\{\int_\Gamma \underline{E}^* \cdot \underline{J}\right\} \geq 0 \tag{15}$$

where superscript * denotes complex conjugate. We obtain in Appendix A the following sufficient uniqueness conditions (SUCs) that imply Eq. (15):

$$\begin{aligned} a_0 \neq 0;\ \ a_1 \neq 0;\ \ a_2 \neq 0: \\ z = 1 - b_1 a_0/a_1 - b_2 a_0/a_2 \\ \text{Re}(a_0) \geq 0;\ \ \text{Re}(a_1) \leq 0;\ \ \text{Re}(a_2) \leq 0 \\ \text{Re}(a_0^* z) \geq 0;\ \ \text{Re}(a_1^* z) \leq 0;\ \ \text{Re}(a_2^* z) \leq 0 \\ \text{Re}(b_1/a_1) \geq 0;\ \ \text{Re}(b_2/a_2) \geq 0 \\ \text{Re}\left(\frac{b_1 a_2^*}{a_1 a_0^*}\right) \leq 0;\ \ \text{Re}\left(\frac{b_2 a_1^*}{a_2 a_0^*}\right) \leq 0 \\ a_1 = a_2 = 0: \\ \text{Re}(a_0) \geq 0;\ \ \text{Re}(a_0^* b_1) \leq 0;\ \ \text{Re}(a_0^* b_2) \leq 0 \end{aligned} \tag{16}$$

Then, if $\mathbb{S}$ denotes the subset of $\mathbb{C}^5$ that satisfies Eq. (16), we have

$$\chi^{LPA} = \text{argmin}_{\chi\in\mathbb{S}} \left\{ \sum_p \int_0^{s_M} \left| Z^p_{ex}(s) - Z^p_{ibc}(s,\chi) \right| ds \right\} \tag{17}$$

for the plane and

$$\chi^{LSA} = \text{argmin}_{\chi\in\mathbb{S}} \left\{ \sum_{n=1}^{N} \left| \alpha^{ex}_n - \alpha^{ibc}_n(\chi) \right| + \left| \beta^{ex}_n - \beta^{ibc}_n(\chi) \right| \right\} \tag{18}$$

for the sphere. Note that, for the plane, Eq. (15) implies $|r^p(s)| \leq 1$ for $s \leq 1$ (theorem 9 in [9]).

3. IMPLEMENTATION OF THE HOIBC IN THE EFIE+MFIE FORMULATION

Let $\underline{M} = \underline{n} \times \underline{E}$ and $g(\underline{r},\underline{r}') = \dfrac{e^{-ik|\underline{r}-\underline{r}'|}}{4\pi|\underline{r}-\underline{r}'|}$. The EFIE and MFIE read for $\underline{r} \in \Gamma$:

$$\begin{aligned}
&EFIE: \ \underline{E}_t(\underline{r})/2 + \mathcal{T}\underline{J}(\underline{r}) - \mathcal{K}\underline{M}(\underline{r}) = \underline{E}^{inc}_t(\underline{r}) \\
&MFIE: \ \underline{H}_t(\underline{r})/2 - \mathcal{T}\underline{M}(\underline{r}) - \mathcal{K}\underline{J}(\underline{r}) = \underline{H}^{inc}_t(\underline{r}) \\
&\mathcal{T}\underline{J}(\underline{r}) = \frac{i}{k}\underline{\nabla}_t \int_\Gamma g(\underline{r},\underline{r}')\underline{\nabla}'\cdot\underline{J}(\underline{r}')\ d\underline{r}' + ik\left[\int_\Gamma g(\underline{r},\underline{r}')\underline{J}(\underline{r}')\ d\underline{r}'\right]_t \\
&\mathcal{K}\underline{M}(\underline{r}) = \left[p.v.\int_\Gamma \underline{\nabla} g(\underline{r},\underline{r}')\times\underline{M}(\underline{r}')\ d\underline{r}'\right]_t
\end{aligned} \tag{19}$$

($p.v.$ stands for principal value). The IBC3 is implemented successively in the EFIE and MFIE. $\underline{J}$ and $\underline{M}$ are discretized in $H(div)$:

$$\underline{J}(\underline{r}) = \sum_{j=1}^{N} I_j \underline{\phi}_j(\underline{r}); \quad \underline{M}(\underline{r}) = \sum_{j=1}^{N} m_j \underline{\phi}_j(\underline{r}) \tag{20}$$

where $\underline{\phi}_j(\underline{r})$ is an RWG basis function, and I_j, m_j are the unknowns, defined on the N edges of the triangular mesh of Γ, of the final global system obtained at the end of this Section.

3.1. Discretization of the EFIE

Eq. (3) entails

$$\underline{E}_t/2 = L_J\underline{J}/2 - (b_1 L_D - b_2 L_R)\underline{E}_t/2 \tag{21}$$

and the EFIE reads

$$(L_J/2 + \mathcal{T})\underline{J} - (b_1 L_D - b_2 L_R)\underline{E}_t/2 - \mathcal{K}\underline{M} = \underline{E}^{inc}_t \tag{22}$$

$\underline{E}_t$ is also discretized in $H(div)$:

$$\underline{E}_t(\underline{r}) = \sum_{j=1}^{N} e_j \underline{\phi}_j(\underline{r}) \tag{23}$$

Then Eq. (22) projected onto the $\{\underline{\phi}_i\}$ basis (i.e., performing the inner product on Γ with $\underline{\phi}_i$) yields

$$\left\{ \frac{1}{2}\left(a_0\mathbf{G} + a_1\mathbf{L^D} - a_2\mathbf{L^R}\right) + \mathbf{T} \right\} \underline{I} - \frac{1}{2}\left(b_1\mathbf{L^D} - b_2\mathbf{L^R}\right)\underline{e} - \mathbf{K}\underline{m} = \underline{b}^E \tag{24}$$

with

$$\begin{aligned}
\mathbf{T}_{ij} &= ik\int_{\Gamma\times\Gamma} g\left(\underline{r},\underline{r}'\right)\underline{\phi}_i\left(\underline{r}\right)\cdot\underline{\phi}_j\left(\underline{r}'\right)d\underline{r}d\underline{r}' - \frac{i}{k}\int_{\Gamma\times\Gamma} g\left(\underline{r},\underline{r}'\right)\underline{\nabla}\cdot\underline{\phi}_i\left(\underline{r}\right)\underline{\nabla}'\cdot\underline{\phi}_j\left(\underline{r}'\right)d\underline{r}d\underline{r}' \\
\mathbf{K}_{ij} &= \int_{\Gamma\times\Gamma}\underline{\phi}_i\left(\underline{r}\right)\cdot\left[\underline{\nabla} g\left(\underline{r},\underline{r}'\right)\times\underline{\phi}_j\left(\underline{r}'\right)\right]d\underline{r}d\underline{r}'
\end{aligned}$$

$$\begin{aligned}
\mathbf{L^D}_{ij} &= \int_\Gamma \underline{\phi}_i \cdot L_D \underline{\phi}_j = -\int_\Gamma \underline{\nabla}_t \cdot \underline{\phi}_i \underline{\nabla}_t \cdot \underline{\phi}_j \\
\mathbf{L^R}_{ij} &= \int_\Gamma \underline{\phi}_i \cdot L_R \underline{\phi}_j = \int_\Gamma \underline{\nabla}_t \cdot \left(\underline{n} \times \underline{\phi}_i\right) \underline{\nabla}_t \cdot \left(\underline{n} \times \underline{\phi}_j\right) \\
\mathbf{G}_{ij} &= \int_\Gamma \underline{\phi}_i \cdot \underline{\phi}_j; \quad b_i^E = \int_\Gamma \underline{\phi}_i\,(\underline{r}) \cdot \underline{E}^{inc}\,(\underline{r})\, d\underline{r}
\end{aligned} \tag{25}$$

($\mathbf{G}$ is the Gram matrix of the RWG basis). The expression of $\mathbf{L^D}_{ij}$ in Eq. (3.1) comes from the definition of L_D in Eq. (1) and integration by parts on Γ. $\mathbf{L^R}_{ij}$ is obtained as follows from the definition of L_R in Eq. (1) and integration by parts:

$$\begin{aligned}
\mathbf{L^R}_{ij} &= -\int_\Gamma \underline{\phi}_i \cdot \left(\underline{n} \times \underline{\nabla}_t curl_\Gamma \underline{\phi}_j\right) = \int_\Gamma \left(\underline{n} \times \underline{\phi}_i\right) \cdot \underline{\nabla}_t curl_\Gamma \underline{\phi}_j \\
&= -\int_\Gamma curl_\Gamma \underline{\phi}_j \underline{\nabla}_t \cdot \left(\underline{n} \times \underline{\phi}_j\right)
\end{aligned} \tag{26}$$

The evaluation of $\mathbf{L^R}_{ij}$ is problematic because $\underline{\nabla}_t \cdot (\underline{n} \times \underline{\phi}_i)$ involves Dirac distributions centered on the edge associated with $\underline{\phi}_i$. Let $\{\underline{p}_i = -\underline{n} \times \underline{\phi}_i\}$ be the $H(curl)$ basis on Γ. As in [11], a simple way to circumvent this difficulty is to use the *curl*2*div* transformation, recalled in Appendix B, that expresses $\underline{p}_i$ in the $\{\underline{\phi}_i\}$ basis and gives (see Appendix B)

$$\mathbf{L^R} = -9\widetilde{\mathbf{G}}^t \mathbf{L^D} \widetilde{\mathbf{G}} \tag{27}$$

From Eqs. (20) and (23) we get

$$\underline{M} = \sum_{j=1}^N m_j \underline{\phi}_j(\underline{r}) = \underline{n} \times \underline{E} = \sum_{j=1}^N e_j \underline{n} \times \underline{\phi}_j = -\sum_{j=1}^N e_j \underline{p}_j \in H(curl) \tag{28}$$

and the *div*2*curl* transformation yields (see Eqs. (B1) and (B2) in Appendix B)

$$\underline{e} = 3\widetilde{\mathbf{G}}\underline{m} \tag{29}$$

Finally, from Eqs. (27) and (29), Eq. (24) reads

$$\left\{\frac{1}{2}\left(a_0\mathbf{G} + a_1\mathbf{L^D} + 9a_2\widetilde{\mathbf{G}}^t\mathbf{L^D}\widetilde{\mathbf{G}}\right) + \mathbf{T}\right\}\underline{I} - \left\{\frac{3}{2}(b_1\mathbf{L^D} + 9b_2\widetilde{\mathbf{G}}^t\mathbf{L^D}\widetilde{\mathbf{G}})\widetilde{\mathbf{G}} + \mathbf{K}\right\}\underline{m} = \underline{b}^E \tag{30}$$

3.2. Discretization of the MFIE

Eq. (3) entails

$$\underline{H}_t/2 = \frac{\underline{n} \times (a_1 L_D - a_2 L_R)\underline{J} - \underline{M} - \underline{n} \times (b_1 L_D - b_2 L_R)\underline{E}_t}{2a_0} \tag{31}$$

Then $\underline{M}$ is discretized as in Eq. (20) and $\underline{E}_t = -\underline{n} \times \underline{M} = \sum_{j=1}^N m_j \underline{p}_j$. $\underline{J}$ is discretized as in Eq. (20) for the $\mathcal{K}\underline{J}(\underline{r})$ term in Eq. (19), and in $H(curl)$ for the $\{\underline{n} \times (a_1 L_D - a_2 L_R)\underline{J}\}$ term:

$$\underline{J}(\underline{r}) = \sum_{j=1}^N I'_j \underline{p}_j(\underline{r}) \tag{32}$$

Then, projecting onto the $\{\underline{\phi}_i\}$ basis, we get

$$\frac{a_1\mathbf{X^D} - a_2\mathbf{X^R}}{2a_0}\underline{I}' - \left\{\frac{\mathbf{G} + b_1\mathbf{X^D} - b_2\mathbf{X^R}}{2a_0} + \mathbf{T}\right\}\underline{m} - \mathbf{K}\underline{I} = \underline{b}^H \tag{33}$$

with

$$\begin{aligned}
\mathbf{X^D}_{ij} &= \int_\Gamma \underline{\phi}_i \cdot \left(\underline{n} \times L_D \underline{p}_j\right) = -\int_\Gamma \underline{\nabla}_t \cdot \underline{p}_i \underline{\nabla}_t \cdot \underline{p}_j \\
\mathbf{X^R}_{ij} &= \int_\Gamma \underline{\phi}_i \cdot \left(\underline{n} \times L_R \underline{p}_j\right) = -\mathbf{L^D}_{ij}; \quad b_i^H = \int_\Gamma \underline{\phi}_i \cdot \underline{H}^{inc}
\end{aligned} \tag{34}$$

The last identity comes from Eq. (4). $\mathbf{X^D}$ is evaluated via the *curl*2*div* transformation (see Eq. (B2) in Appendix B)

$$\mathbf{X^D} = 9\widetilde{\mathbf{G}}^t\mathbf{L^D}\widetilde{\mathbf{G}} \tag{35}$$

and (Eqs. 32) and (20) yield, with the *div*2*curl* transformation,

$$\underline{I}' = -3\widetilde{\mathbf{G}}\underline{I}$$

so that the MFIE reads

$$\left\{\frac{3}{2a_0}\left(9a_1\widetilde{\mathbf{G}}^t\mathbf{L^D}\widetilde{\mathbf{G}} + a_2\mathbf{L^D}\right)\widetilde{\mathbf{G}} + \mathbf{K}\right\}\underline{I} + \left\{\frac{1}{2a_0}\left(\mathbf{G} + 9b_1\widetilde{\mathbf{G}}^t\mathbf{L^D}\widetilde{\mathbf{G}} + b_2\mathbf{L^D}\right) + \mathbf{T}\right\}\underline{m} = -\underline{b}^H \tag{36}$$

Finally, Eqs. (30) and (36) yield the system

$$\begin{aligned}
&(\mathbf{A}+\mathbf{B})\underline{x} = \underline{b};\quad \underline{x} = (\underline{I},\underline{m})^t;\quad \underline{b} = (\underline{b}^E,\underline{b}^H)^t\\
&\mathbf{A} = \begin{pmatrix} \dfrac{a_0\mathbf{G}}{2} + \mathbf{T} & \mathbf{K} \\ \mathbf{K} & \dfrac{\mathbf{G}}{2a_0} + \mathbf{T} \end{pmatrix}\\
&\mathbf{B} = \begin{pmatrix} \dfrac{a_1\mathbf{L^D} + 9a_2\widetilde{\mathbf{G}}^t\mathbf{L^D}\widetilde{\mathbf{G}}}{2} & \dfrac{3(b_1\mathbf{L^D} + 9b_2\widetilde{\mathbf{G}}^t\mathbf{L^D}\widetilde{\mathbf{G}})\widetilde{\mathbf{G}}}{2} \\ \dfrac{3(9a_1\widetilde{\mathbf{G}}^t\mathbf{L^D}\widetilde{\mathbf{G}} + a_2\mathbf{L^D})\widetilde{\mathbf{G}}}{2a_0} & \dfrac{9b_1\widetilde{\mathbf{G}}^t\mathbf{L^D}\widetilde{\mathbf{G}} + b_2\mathbf{L^D}}{2a_0} \end{pmatrix}
\end{aligned} \tag{37}$$

($\mathbf{A}$ is symmetric). It is demonstrated in Appendix C that Eq. (37) has a unique solution if the SUCs are satisfied with the additional constraint

$$\mathrm{Re}(a_0) \geq \epsilon_\delta > 0 \tag{38}$$

Note that when $a_1 = a_2 = b_1 = b_2 = 0$ we recover the system $\mathbf{A}\underline{x} = \underline{b}$ proposed in [14] for the IBC0 that has been proved to be well-posed if $\mathrm{Re}(a_0) > 0$.

4. NUMERICAL RESULTS

Unlike the IBCs obtained in [2–4] for a thin monolayer, the range of validity of the essentially heuristic IBC3 must be numerically evaluated. Such an evaluation has already been performed in [7] by considering the plane and the 2D circular cylinder. We have now another canonical geometry at our disposal, the sphere considered in Section 2.2. Regarding the plane, we set here $s_M = 1.2$ because the contribution to the RCS of the far-field radiated by an evanescent surface wave ($s > 1$) is all the smallest as s is larger than one [22]. First, following [7], we consider in Section 4.1 a monolayer that illustrates some of the main problems encountered by the IBC3. Without loss of generality, we have set $Z_b = 0$ in all that follows (PEC backed coating), and h designates the average edge length h of a mesh of Γ. The IBC3 coefficients are always obtained with the SUCs that degrade only slightly the IBC performances, unlike the ones proposed in [11]. The errors made on the impedance (for the plane) and the RCS (for a 3D object) are measured by

$$\begin{aligned}
err_Z &= \max_{p=TM,TE}\sqrt{\frac{\displaystyle\int_0^{s_M}\left|Z^p_{ex}(s) - Z^p_{ibc}(s)\right|^2 ds}{\displaystyle\int_0^{s_M}\left|Z^p_{ex}(s)\right|^2 ds}}\\
err_{RCS}(dB) &= \max_{p=TM,TE}\frac{1}{\pi}\int_0^{\pi}\left|RCS^p(\theta) - RCS^p_{ex}(\theta)\right| d\theta
\end{aligned} \tag{39}$$

The various coatings that are considered are listed in Table 1.

Table 1. PEC backed coatings. $n_i = |\sqrt{\epsilon_i \mu_i}|$ is the material index in layer i (for a multilayer $i = 1$ designates the innermost layer).

	i	d_i(cm)	ϵ_i	μ_i	n_i
TEST1	1	5	4	1	2
TEST2	1	7.5	1	7.5	2.74
TEST3	1	5	1-i	(1-i)/2	1
TEST4	1	1	1-i	(1-i)/2	1
	2	1	2-i	1/2	1.06
	3	1	1/2	2-i	1.06
TEST5	1	1	4-i	2-i/2	2.9
	2	1	4-i	2-i	3.04
	3	1	2-i	4-i	3.04

4.1. Lossless Monolayer with Thickness *d*

In this Section $f = 1\,\text{GHz}$ unless otherwise specified. The TEST1 coating considered in [7] is difficult to model for two reasons: it supports surface waves (SWs) for $s = s_r > 1$ and Z_{ex}^p has an asymptote for $s = s_\infty$. The numerically derived values of s_r [22] are 1.06 in TE and 1.56 in TM that yield $|r_{ex}^p(s_r)| = \infty$, as observed in Fig. 1 ($s_M = 2$ in Figs. 1, 2). Also, we have [7, 8]

$$Z_{ex}^{TM} = \frac{i\sqrt{\epsilon\mu - s^2}}{\epsilon} \tan\left(kd\sqrt{\epsilon\mu - s^2}\right); \quad Z_{ex}^{TE} = \frac{i\mu}{\sqrt{\epsilon\mu - s^2}} \tan\left(kd\sqrt{\epsilon\mu - s^2}\right) \tag{40}$$

that entails there exists q integer such that

$$s_\infty = \sqrt{\epsilon\mu - \left[\frac{(2q+1)\pi}{2kd}\right]^2} \tag{41}$$

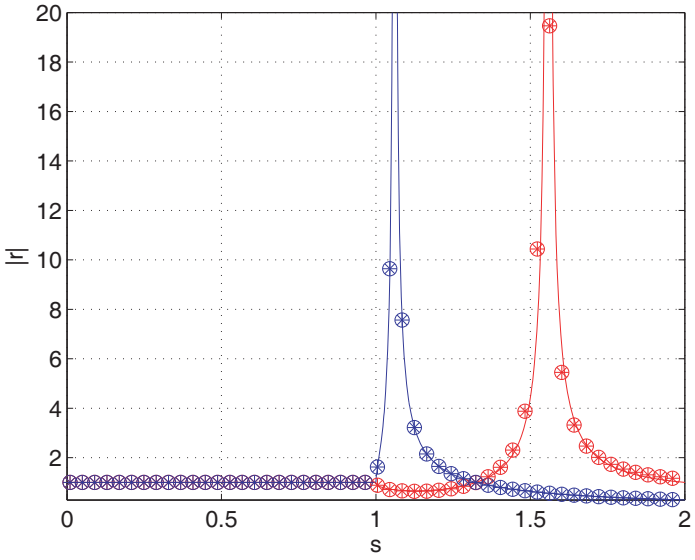

Figure 1. TEST1, IBC3 with $s_M = 2$, plane. Modulus of the reflection coefficient vs. s. Red (blue): TM (TE). Solid line: $|r_{ex}^p|$; circles: $|r_{ibc}^p|$ without SUCs; stars: $|r_{ibc}^p|$ with SUCs. The resonances at $s_r = 1.06$ (TE) and $s_r = 1.56$ (TM) due to the SWs ($|r_{ex}^p(s_r)| = \infty$) are accurately accounted for by the IBC3.

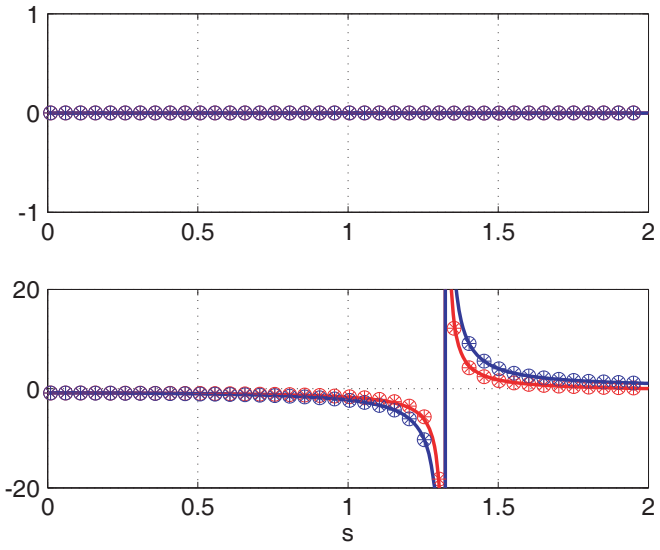

Figure 2. TEST1, IBC3 with $s_M = 2$, plane, Z^p_{ex}, $Z^p_{ibc}(s)$, p =TM (red) or TE (blue). Top (bottom): $Re(Z)$ ($Im(Z)$ respectively). Solid line: Z^p_{ex}; circles: Z^p_{ibc} without SUCs; stars: Z^p_{ibc} with SUCs. The IBC0 yields $Z^{TM}(s) = Z^{TE}(s) = 0.0772 + 0.126i$. The asymptote at $s_\infty = 1.32$ is well reproduced by the IBC3.

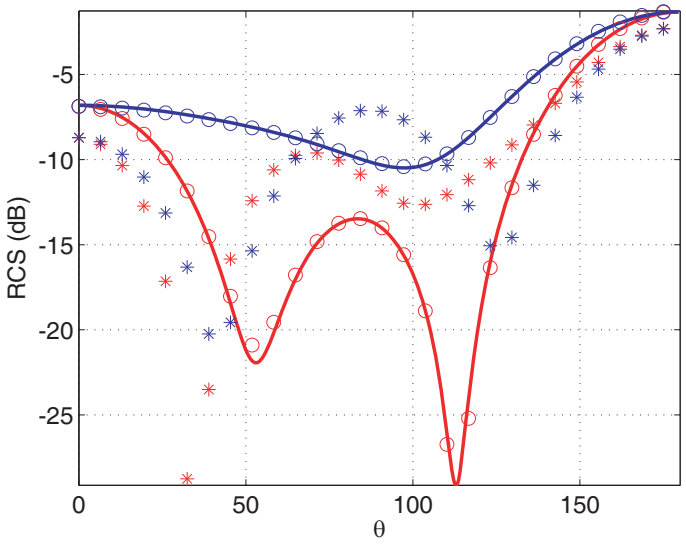

Figure 3. TEST1, sphere $R = 5cm$, IBC3. RCS vs. θ. Red (blue): TM (TE). Solid line: exact; circles: LSA (Eq. 18); stars: LPA (Eq. 17). These plots highlight the improved accuracy achieved by the IBC3 when its coefficients take into account the curvature of the sphere (here $1/kR = 0.954$).

and $s_\infty(q = 0) = 1.32$, as observed in Fig. 2. These plots demonstrate the high efficiency achieved by the IBC3. In view of Eq. (10), the asymptote is reproduced by the IBC3 if $b_1 = b_2 = 1/(ks_\infty)^2 \in \mathbb{R}$ that is actually verified here: Eq. (17) yields $b_1 = b_2 = 0.5703/k^2$. Fig. 3 plots the RCS of a $R = 5\,\text{cm}$ sphere computed with the LPA-IBC3 and LSA-IBC3: it confirms that the LPA is all the less satisfied since the electric curvatures of the surface are large. For the same sphere, Figs. 4 and 5 illustrate the superior results obtained for the scattered electric near-field when the LSA-IBC3 is employed in lieu of the LSA-IBC0. Also, as expected, we have verified that the IBC0, IBC02 and IBC1 yield large impedance errors (see the TEST1 results in Table 2). Finally, this example illustrates the inability of the

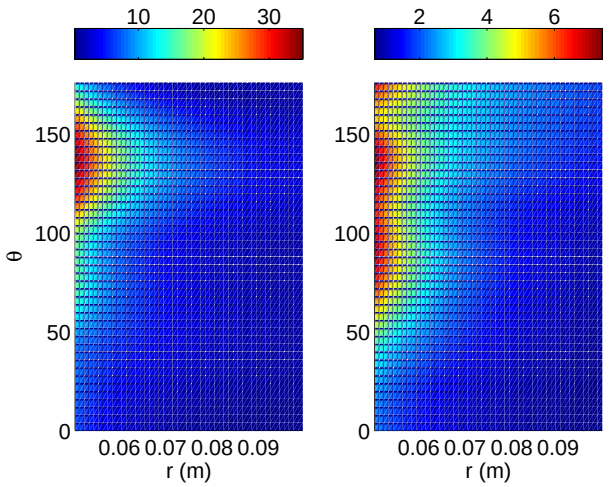

Figure 4. Sphere $R = 5\,\mathrm{cm}$, TEST1, $\theta = 0$ incidence. Modulus of the scattered near-field $\underline{E}^s(r, \theta, \phi = 0)$ in V/m. Left: exact; right: IBC0 (LSA).

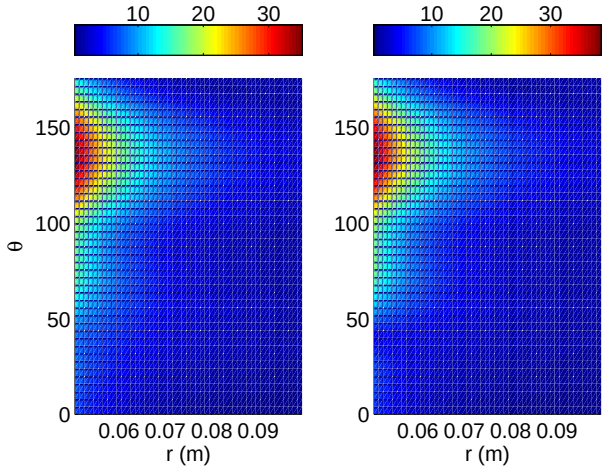

Figure 5. Sphere $R = 5cm$, TEST1, $\theta = 0$ incidence. Modulus of the scattered near-field $\underline{E}^s(r, \theta, \phi = 0)$ in V/m. Left: exact; right: IBC3 (LSA).

EFIE+MFIE formulation (37) to model this lossless coating: because Eq. (40) implies $\mathrm{Re}(Z^p_{ex})(s) = 0$ for $s \leq \sqrt{\epsilon\mu} \leq 2$ we get from Eq. (10) $\mathrm{Re}(a_0) = Re(a_1) = \mathrm{Re}(a_2) = 0$, and constraint (38) is violated. As a result, we have found that the numerical solution of Eq. (37) is erroneous even with a dense mesh of Γ since the condition number of matrix $(\mathbf{A} + \mathbf{B})$ increases when h decreases. Also, we have observed that (i) increasing ϵ_δ reduces drastically the IBC3 efficiency and (ii) the same behaviour is obtained with the unconstrained IBC3 that yields $Re(a_0) = -6.10^{-5}$.

As d is increased, more SWs appear: $d = 10\,\mathrm{cm}$ yields three SWs ($s_r^{TM} = 1.023$ and 1.875; $s_r^{TE} = 1.636$) and the impedance is infinite for $s_\infty = 1.86$. Since only the first TM wave contributes to the RCS, $s_M = 1.2$ is sufficient that yields $err_Z(s_M = 1.2) = 0.84\%$. If, as in [7], s_M is larger, the error increases ($err_Z(s_M = 1.8) = 21\%$). This is due to the fact that additional coefficients are needed to model accurately the exact impedance. A way to introduce these extra coefficients is to add in the HOIBC powers of the L_D and L_R operators as it has been done in, e.g., [27] with the drawback of increasing the number of unknowns in the final system for discretization purposes.

We consider now the TEST2 coating tested on a 2D cylinder in [7] where it is shown that the LPA-IBC3 cannot model a resonant circumferential wave on the cylinder. We put this coating on a

$R = 30\,\text{cm}$ sphere with $d = 7.5\,\text{cm} = \lambda_0/4$. For $f = 1.053\,\text{GHz}$, a whispering gallery wave (WGW) propagates on the inside of Γ. A WGW corresponds with a very sharp electromagnetic resonance inside the coating and is responsible for strong echos of long duration in time that may alter considerably the RCS of a stealth object [25, 26]. Following [26], we have numerically obtained $f_r = 1.053 + i2.5\,10^{-4}$ (in GHz) for the complex frequency that yields the strongest resonance, i.e., the smallest $\text{Im}(f_r)$, and the WGW propagates along a meridian of the sphere with a phase velocity $v_\phi = 0.66c$ larger than $c/\sqrt{\epsilon\mu} = 0.365c$ as expected [26]. Since WGWs propagate on curved surfaces only, they are taken into account by the IBC3 when the coefficients are calculated on the spherical coating only, as demonstrated in Fig. 6 where $err_{RCS}(s_M = 1.2) = 0.01\,\text{dB}$ for the LSA-IBC3 while $err_{RCS}(s_M = 1.2) = 3.8\,\text{dB}$ for the LPA-IBC3.

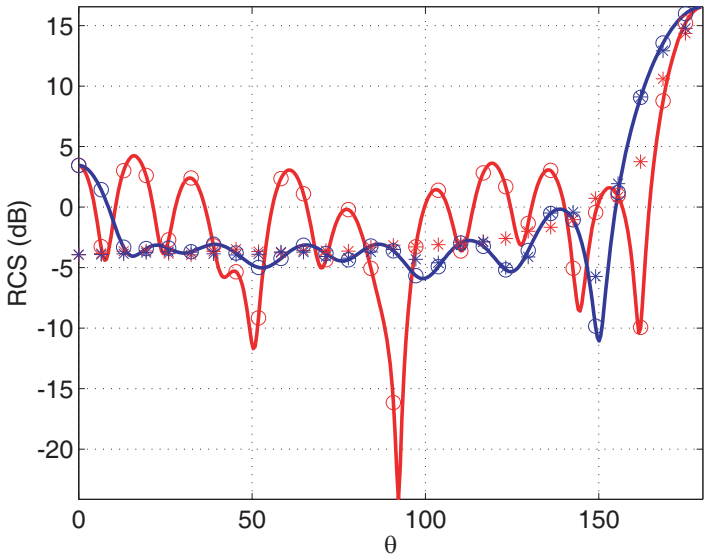

Figure 6. TEST2, sphere $R = 30cm$, $f = 1.053GHz$, IBC3. RCS vs. θ. Red (blue): TM (TE). Solid line: exact; circles: LSA (Eq. 18); stars: LPA (Eq. 17). f is close to the complex resonance frequency $f_r = 1.053 + i2.5\,10^{-4}$ of a WGW that cannot be accounted for by the LPA-IBC3.

In view of these results, which can be extended to a multilayer coating, we propose the following rules relative to the use of the IBC3 in lieu of a more expensive numerical approach. First, measure the IBC3 performances on the planar coating for $s \in [0, s_M]$, as indicated in Section 2.2.1, with $s_M \simeq 1.2$; a larger value of s_M (say $s_M = 1.5$) might be required for a stealth object, as explained in [22]. A sphere whose radius is one of the local radii of curvature of the 3D object upon which the IBC3 is to be implemented can serve to evaluate the pertinence of the LPA (see Section 2.2.2). Then, if at least one layer has very small losses ($|\text{Im}(\epsilon)/\epsilon|, |\text{Im}(\mu)/\mu| \ll 1$, strong resonances may exist (SW, WGW) and caution is required. If a SW is involved, the previous procedure can be applied; however, ϵ_δ in constraint (38) may be close to zero, and the EFIE+MFIE formulation might be numerically ill-posed. If a WGW exists there is no effective solution since the corresponding resonance cannot be reproduced on a planar coating; the sphere might help but a WGW resonance is shape dependent.

4.2. Bodies of Revolution (BORs)

A BOR hybrid finite element-integral equation numerical code [23] serves as a reference. The solution of Eq. (37) is obtained with a direct solver (standard Gaussian elimination) and

$$Q = \max_p \left\{ \text{Re} \int_\Gamma \underline{J}^{p*}(\underline{r}) \cdot \underline{E}^p(\underline{r})\, d\underline{r} \right\} \tag{42}$$

is computed numerically that has always been found non negative, in accordance with Eq. (15). The performances of the various IBCs are indicated in Table 2 for the TEST3, TEST4, TEST5 coatings

Figure 7. Cylinder (length 2 m) with hemispherical caps (radius 25 cm).

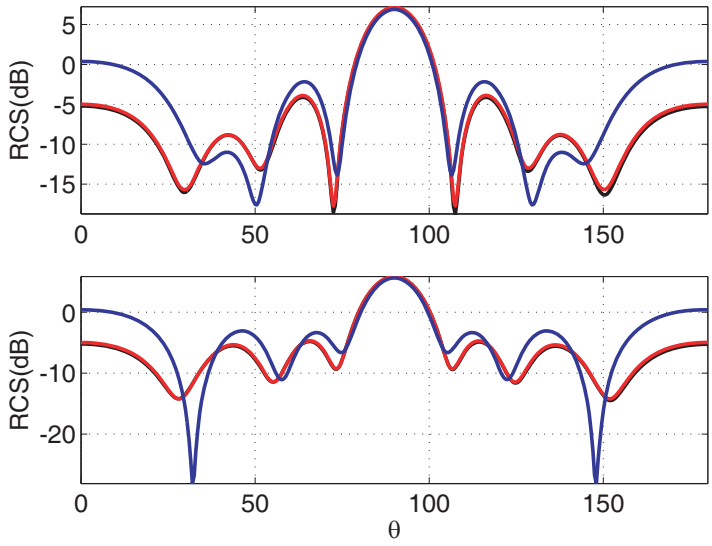

Figure 8. EFIE+MFIE. Monostatic RCS of the cylinder in Fig. 7, 200 MHz, 7240 triangles ($h = \lambda_0/23$), TEST3 coating. Top (bottom): TM (TE). Black: reference; red: IBC3; blue: IBC0. Reference and LPA-IBC3 RCSs are superimposed.

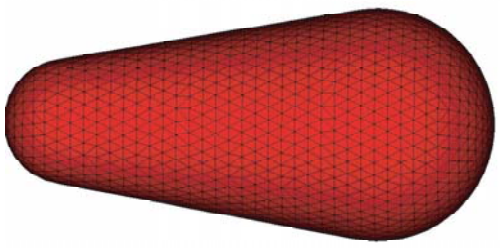

Figure 9. Cone-sphere with rounded tip. Total length of the PEC surface 48.55 cm, tip radius 4 cm, sphere radius 10 cm.

considered here. First, the RCS of the cylinder in Fig. 7 with the low index TEST3 monolayer is plotted for $f = 200$ MHz in Fig. 8. Then, the RCS of the cone-sphere in Fig. 9 is computed for the low index TEST4 (Fig. 10) and the larger index TEST5 (Fig. 11) coatings with the IBC0 and the IBC3 with the LPA coefficients (i) on the whole surface and (ii) everywhere except on the back sphere where they are replaced by the LSA coefficients calculated on the sphere with the same 10 cm radius. All these plots demonstrate the superiority of the IBC3 over the IBC0 when the coating index is small. Also, the LSA-IBC3 on the back sphere increases but slightly the IBC3 performances (see Table 3) because the LPA-IBC3 is already fairly accurate. Note that err_{RCS} obtained on the TEST5 sphere in Table 3 with the LSA is larger than with the LPA. This may happen with the SUCs in Eq. (16) since χ in Eq. (18) spans a smaller parameter space: actually $err_{RCS} = 0.0073$ when χ is unconstrained.

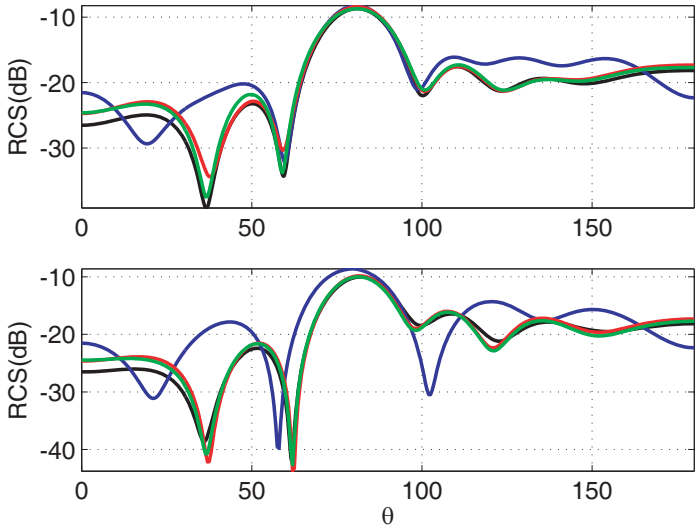

Figure 10. EFIE+MFIE. Monostatic RCS of the cone-sphere in Fig. 9, 1 GHz, 3472 triangles ($h = \lambda_0/19$), TEST4 coating. Top (bottom): TM (TE). Black: reference; blue: IBC0; red: LPA-IBC3; green: LSA-IBC3 on the back sphere and LPA-IBC3 elsewhere.

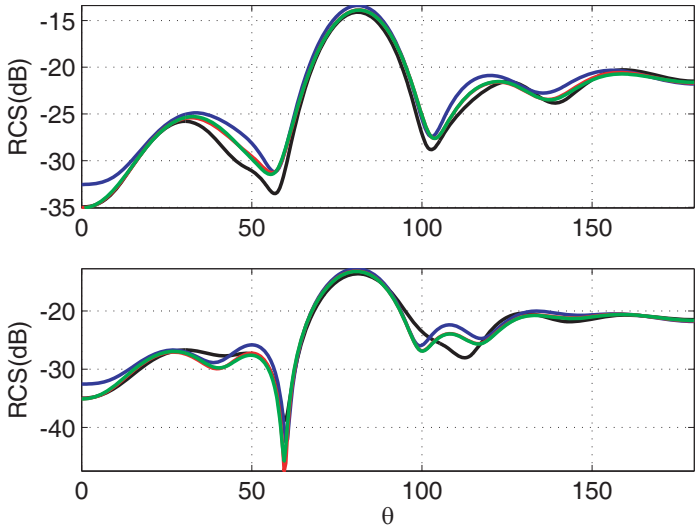

Figure 11. EFIE+MFIE. Monostatic RCS of the cone-sphere in Fig. 9, TEST5 coating. Same captions as in Fig. 10.

Table 2. LPA with $s_M = 1.2$. Discrepancy err_Z (in percent), as defined in Eq. (39), between the exact and approximate impedances.

	IBC0	IBC02		IBC1		IBC3	
		wo. SUC	SUC	wo. SUC	SUC	wo. SUC	SUC
TEST1	66.3	22.6	22.6	45.2	45.2	0.48	0.48
TEST3	44.3	2.8	11.6	48.7	66.5	0.08	3.6
TEST4	73.1	1.2	1.9	71.7	98	0.02	1.5
TEST5	9.3	0.4	4.8	44	35.6	0.008	0.3

Table 3. Discrepancy err_{RCS} (in dB), as defined in Eq. (39), between the exact and approximate RCSs for the cone-sphere and the sphere with the same radius as the back sphere.

	cone-sphere			sphere $R = 10\,\text{cm}$	
	IBC0	LPA-IBC3 everywhere	LSA-IBC3 on the back sphere	LPA-IBC3	LSA-IBC3
TEST4	4.34	1.05	0.84	0.48	0.035
TEST5	1.17	0.82	0.81	0.26	0.49

5. CONCLUSIONS

The numerical examples that have been presented demonstrate that the IBC3, even constrained by the new SUCs presented in Section 2.3, is superior to the Leontovich IBC0, especially when the material index is small. However, it remains an approximation whose efficiency can be straightforwardly estimated a priori from the reflection coefficient calculated either on a plane (LPA) or on a sphere (LSA). Its range of validity has been discussed, and it has been shown that resonant circumferential waves, such as WGWs, can be accounted for if the IBC3 coefficients are calculated on a curved surface only, as it has been done for the sphere in Section 2.2. The numerical implementation of the IBC3 in the EFIE+MFIE formulation has been facilitated by the *div*2*curl* and *curl*2*div* transformations. It has been shown that this particular EFIE+MFIE formulation is well posed if the SUC in Eq. (38) is added. This SUC is specific to this formulation and is not required if the IBC3 is implemented in, e.g., a finite element method to model heterogeneous structures layed over a multilayer. Finally, it is noteworthy that the IBC3 can be applied to more complex structures, such as metamaterials (as it has been done for the FSSs in [27, 28]), provided that their exact reflection coefficient is known.

APPENDIX A. DERIVATION OF THE SUCS IN (16)

If $\text{Re}(a_0) \geq 0$, $\text{Re}(a_1) \leq 0$, $\text{Re}(a_2) \leq 0$, operators $a_0 + a_1 L_D$, $a_0 - a_2 L_R$ and L_J are injective on account of the well-known identities

$$\int_\Gamma \underline{V}_t^* \cdot L_D \underline{V}_t = -\int_\Gamma |\underline{\nabla}_t \cdot \underline{V}_t|^2; \quad \int_\Gamma \underline{V}_t^* \cdot L_R \underline{V}_t = \int_\Gamma |\underline{n} \cdot \underline{curl}_t \underline{V}_t|^2 \tag{A1}$$

Then Eq. (15) yields

$$X = \int_\Gamma \underline{E}^* \cdot \underline{J} = \int_\Gamma \left[L_J^{-1} + b_1 L_J^{-1} L_D - b_2 L_J^{-1} L_R\right] \underline{E} \cdot \underline{E}^*$$

Because $L_D = (a_0 + a_1 L_D - a_0)/a_1$ and $L_R = -(a_0 - a_2 L_R - a_0)/a_2$ we get

$$X = \int_\Gamma \left[\left(1 - \frac{b_1 a_0}{a_1} - \frac{b_2 a_0}{a_2}\right) L_J^{-1} + \frac{b_1}{a_1} L_J^{-1}(a_0 + a_1 L_D) + \frac{b_2}{a_2} L_J^{-1}(a_0 - a_2 L_R)\right] \underline{E} \cdot \underline{E}^*$$

We set $\underline{D} = L_J^{-1}\underline{E}$ ($\Longrightarrow \underline{E} = L_J \underline{D}$) and identities $L_J^{-1}(a_0 + a_1 L_D) = [1 - a_2(a_0 + a_1 L_D)^{-1} L_R]^{-1}$, $L_J^{-1}(a_0 - a_2 L_R) = [1 + a_1(a_0 - a_2 L_R)^{-1} L_D]^{-1}$ yield

$$\begin{aligned} X &= \int_\Gamma \left[\left(1 - \frac{b_1 a_0}{a_1} - \frac{b_2 a_0}{a_2}\right) D_0 + \frac{b_1}{a_1} \underline{E}^* \cdot \underline{D}_1 + \frac{b_2}{a_2} \underline{E}^* \cdot \underline{D}_2\right] \\ D_0 &= \underline{D} \cdot (L_J \underline{D})^*; \quad \underline{D}_1 = \left[1 - a_2(a_0 + a_1 L_D)^{-1} L_R\right]^{-1} \underline{E} \\ \underline{D}_2 &= \left[1 + a_1(a_0 - a_2 L_R)^{-1} L_D\right]^{-1} \underline{E} \end{aligned} \tag{A2}$$

Substituting $[1-a_2(a_0+a_1L_D)^{-1}L_R]\underline{D}_1$ and $[1+a_1(a_0-a_2L_R)^{-1}L_D]\underline{D}_2$ to $\underline{E}$ in the above expression of X gives

$$\begin{aligned} X &= \int_\Gamma \left\{ \left(1-\frac{b_1a_0}{a_1}-\frac{b_2a_0}{a_2}\right) D_0 + \frac{b_1}{a_1}\underline{D}_1\cdot\left[1-a_2^*(a_0^*+a_1^*L_D)^{-1}L_R\right]\underline{D}_1^* \right. \\ &\quad \left. + \frac{b_2}{a_2}\underline{D}_2\cdot[1+a_1^*(a_0^*-a_2^*L_R)^{-1}L_D]\underline{D}_2^* \right\} \\ &= \int_\Gamma \left\{ \left[\left(1-\frac{b_1a_0}{a_1}-\frac{b_2a_0}{a_2}\right) D_0 + \frac{b_1}{a_1}|\underline{D}_1|^2 + \frac{b_2}{a_2}|\underline{D}_2|^2 - \frac{b_1a_2^*}{a_1}\underline{D}_1\cdot\underline{D}_3 + \frac{b_2a_1^*}{a_2}\underline{D}_2\cdot\underline{D}_4 \right\} \right. \end{aligned} \quad \text{(A3)}$$

where

$$\underline{D}_3 = (a_0^*+a_1^*L_D)^{-1}L_R\underline{D}_1^*; \quad \underline{D}_4 = (a_0^*-a_2^*L_R)^{-1}L_D\underline{D}_2^* \quad \text{(A4)}$$

Eq. (A4) yields $L_R\underline{D}_1^* = (a_0^*+a_1^*L_D)\underline{D}_3$ and, from $L_DL_R = L_RL_D = 0$, $(a_0^*+a_1^*L_D)L_D\underline{D}_3 = 0$ that implies, because $a_0^*+a_1^*L_D$ is injective, $L_D\underline{D}_3 = 0$ and hence $L_R\underline{D}_1^* = a_0^*\underline{D}_3$, so that $\underline{D}_1\cdot\underline{D}_3 = \dfrac{\underline{D}_1\cdot L_R\underline{D}_1^*}{a_0^*}$. Following along the same lines we get $\underline{D}_2\cdot\underline{D}_4 = \dfrac{\underline{D}_2\cdot L_D\underline{D}_2^*}{a_0^*}$, and Eq. (A3) finally reads

$$X = \int_\Gamma \left\{ \left(1-\frac{b_1a_0}{a_1}-\frac{b_2a_0}{a_2}\right) D_0 + \frac{b_1}{a_1}|\underline{D}_1|^2 + \frac{b_2}{a_2}|\underline{D}_2|^2 - \frac{b_1a_2^*}{a_1a_0^*}\underline{D}_1\cdot L_R\underline{D}_1^* + \frac{b_2a_1^*}{a_2a_0^*}\underline{D}_2\cdot L_D\underline{D}_2^* \right\} \quad \text{(A5)}$$

with, from the definition of D_0 in Eq. (A2), $D_0 = a_0^*|\underline{D}|^2 + a_1^*\underline{D}\cdot L_D\underline{D}^* - a_2^*\underline{D}\cdot L_R\underline{D}^*$. The SUCs are then easily deduced from Eq. (A5) on account of Eq. (A1).

APPENDIX B. OVERVIEW OF THE *div2curl* AND *curl2div* TRANSFORMATIONS [10, 11, 17]

For $\underline{r}(\xi_1,\xi_2)$ in triangle T with $(\xi_1,\xi_2)\in[0,1]\times[0,1]$, the RWG functions are defined as

$$\begin{aligned} &\underline{\phi}_i(\underline{r}) = [\psi_{i1}(\xi_1,\xi_2)\underline{e}_1 + \psi_{i2}(\xi_1,\xi_2)\underline{e}_2]/s; \ s = |\underline{e}_1\times\underline{e}_2| \\ &\psi_{11} = \xi_1; \quad \psi_{12} = \xi_2 - 1 \\ &\psi_{21} = \xi_1; \quad \psi_{22} = \xi_2 \\ &\psi_{31} = \xi_1 - 1; \quad \psi_{32} = \xi_2 \end{aligned}$$

$1\le i\le 3$ is the local edge number (see Fig. B1). Also, let $\{\underline{q}_i\}$ be the basis introduced in [14]:

$$\begin{aligned} &\underline{q}_1 = (2\xi_2-1)\underline{e}_1/s; \quad \underline{q}_2 = (1-2(\xi_1+\xi_2))(\underline{e}_2-\underline{e}_1)/s \\ &\underline{q}_3 = (1-2\xi_1)\underline{e}_2/s \end{aligned}$$

(note that $\underline{\nabla}.\underline{q}_i = 0$). Regarding the *div2curl* transformation, let $\underline{c}^i$ be the unknown components of $\underline{\phi}_i$ in the $\{\underline{p}_j = -\underline{n}\times\underline{\phi}_j\}$ $H(curl)$ basis

$$\underline{\phi}_i = \sum_{j=1}^N d_j^i\underline{\phi}_j \simeq \sum_{j=1}^N c_j^i\underline{p}_j; \quad d_j^i = \delta_{ij} \quad \text{(B1)}$$

(δ_{ij} is the Kronecker symbol). We force the projection of Eq. (B1) onto $\{\underline{q}_i\}$ to be equal, i.e., $\sum_{j=1}^N d_j^i\int_\Gamma \underline{q}_i\cdot\underline{\phi}_j = \sum_{j=1}^N c_j^i\int_\Gamma \underline{q}_i\cdot\underline{p}_j$, to obtain

$$\underline{c}^i = -\widehat{\mathbf{G}}^{-1}\widetilde{\mathbf{G}}\underline{d}^i = -3\widetilde{\mathbf{G}}\underline{d}^i \quad \text{(B2)}$$

with

$$\widetilde{\mathbf{G}}_{ij} = -\int_\Gamma \underline{q}_i\cdot\underline{\phi}_j; \quad \widehat{\mathbf{G}}_{ij} = \int_\Gamma \underline{q}_i\cdot\underline{p}_j \quad \text{(B3)}$$

$\widehat{\mathbf{G}}$ is diagonal, $\widehat{\mathbf{G}}^{-1} = 3\mathbf{Id}$ ($\mathbf{Id}$ is the identity) and the elementary matrix corresponding to the triangle in Fig. B1 is

$$\widetilde{\mathbf{G}} = \frac{1}{6s}\begin{pmatrix} |\underline{e}_1|^2/2 - \underline{e}_1.\underline{e}_2 & |\underline{e}_1|^2/2 & -|\underline{e}_1|^2/2 \\ -|\underline{e}_1 - \underline{e}_2|^2/2 & (|\underline{e}_1|^2 - |\underline{e}_2|^2)/2 & |\underline{e}_1 - \underline{e}_2|^2/2 \\ |\underline{e}_2|^2/2 & -|\underline{e}_2|^2/2 & -|\underline{e}_2|^2/2 + \underline{e}_1.\underline{e}_2 \end{pmatrix}$$

($\widetilde{\mathbf{G}}$ is singular). Substituting $\sum_{k=1}^{N} c_k^i \underline{p}_k$ to $\underline{\phi}_i$ and $\sum_{k'=1}^{N} c_{k'}^j \underline{p}_{k'}$ to $\underline{\phi}_j$ in the expression of $\mathbf{L^R}$ in Eq. (3.1) yields Eq. (27). For the *curl*2*div* transformation we have

$$\underline{p}_i = \sum_{j=1}^{N} c_j^i \underline{p}_j \simeq \sum_{j=1}^{N} d_j^i \underline{\phi}_j \ ; \ c_j^i = \delta_{ij} \tag{B4}$$

Again, we force the projection of Eq. (B4) onto $\{\underline{n} \times \underline{q}_i\}$ to be equal to obtain

$$\underline{d}^i = 3\widetilde{\mathbf{G}}\underline{c}^i \tag{B5}$$

Now, $\mathbf{L^R}_{ij}$ in Eq. (3.1) reads $\mathbf{L^R}_{ij} = \int_\Gamma \underline{\nabla}_t \cdot \underline{p}_i \underline{\nabla}_t \cdot \underline{p}_j = -\sum_{kk'} d_k^i d_{k'}^j \mathbf{L^D}_{kk'}$ with, on account of Eq. (B5), $d_k^i = 3\widetilde{\mathbf{G}}_{ki}$ and $d_{k'}^j = 3\widetilde{\mathbf{G}}_{jk'}$, and Eq. (27) is obtained.

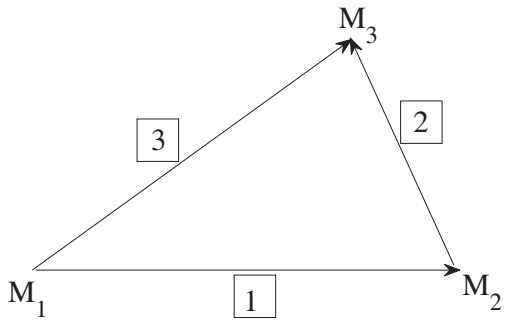

Figure B1. $T = (M_1, M_2, M_3)$: $\underline{e}_1 = \underline{M_1M_2}$, $\underline{e}_2 = \underline{M_1M_3}$, $\underline{n} = \underline{e}_1 \times \underline{e}_2$. Figures inside squares are the local edge numbers.

APPENDIX C. SYSTEM (30) AND (36) HAS A UNIQUE SOLUTION IF THE SUCS ARE SATISFIED AND $\mathbf{Re}(a_0) \neq 0$

Let $\underline{J} = \underline{n} \times \underline{H}$ and $\underline{M} = \underline{n} \times \underline{E}$ be the solutions of Eq. (19) with $\underline{E}^{inc} = \underline{H}^{inc} = 0$ and $\underline{r} \in \Gamma$

$$\underline{E}_t(\underline{r})/2 = -\mathcal{T}\underline{J}(\underline{r}) + \mathcal{K}\underline{M}(\underline{r}) \ ; \ \underline{H}_t(\underline{r})/2 = \mathcal{T}\underline{M}(\underline{r}) + \mathcal{K}\underline{J}(\underline{r}) \tag{C1}$$

$\underline{E}_t$ and $\underline{H}_t$ satisfy the IBC3, viz Eqs. (21) and (31). We look for sufficient conditions on the IBC3 coefficients that imply $\underline{J} = \underline{M} = 0$. Let $\mathbb{T}$ and $\mathbb{K}$ be the operators defined for $\underline{r} \in \mathbb{R}^3$ by

$$\begin{aligned} \mathbb{T}\underline{J}(\underline{r}) &= \frac{i}{k}\underline{\nabla}\int_\Gamma g(\underline{r},\underline{r}')\underline{\nabla}' \cdot \underline{J}(\underline{r}')\ d\underline{r}' + ik\int_\Gamma g(\underline{r},\underline{r}')\underline{J}(\underline{r}')\ d\underline{r}' \\ \mathbb{K}\underline{M}(\underline{r}) &= \int_\Gamma \underline{\nabla} g(\underline{r},\underline{r}') \times \underline{M}(\underline{r}')\ d\underline{r}' \end{aligned} \tag{C2}$$

and $\widehat{\underline{E}}$, $\widehat{\underline{H}}$ the fields defined for $\underline{r} \in \mathbb{R}^3$ by

$$\widehat{\underline{E}}(\underline{r}) = -\mathbb{T}\underline{J}(\underline{r}) + \mathbb{K}\underline{M}(\underline{r}); \quad \widehat{\underline{H}}(\underline{r}) = \mathbb{T}\underline{M}(\underline{r}) + \mathbb{K}\underline{J}(\underline{r}) \tag{C3}$$

The well-known jump identity

$$\mathbb{K}_t\underline{M}\left(\underline{r}^{\pm}\right) = \mathcal{K}\underline{M}\left(\underline{r}\right) \mp \underline{n} \times \underline{M}/2; \quad \mathbb{K}_t\underline{J}\left(\underline{r}^{\pm}\right) = \mathcal{K}\underline{J}\left(\underline{r}\right) \mp \underline{n} \times \underline{J}/2 \tag{C4}$$

with $\underline{r}^{\pm} = \lim_{\epsilon \to 0} \underline{r} \pm \epsilon \underline{n}(\underline{r})$ for $\underline{r} \in \Gamma$, the continuity of $\mathbb{T}_t \underline{J} = \mathcal{T}\underline{J}$, $\mathbb{T}_t \underline{M} = \mathcal{T}\underline{M}$ on Γ and Eq. (C1) yield

$$\begin{aligned} \widehat{\underline{E}}_t(\underline{r}^-) &= -\mathcal{T}\underline{J} + \mathcal{K}\underline{M} + \underline{n} \times \underline{M}/2 = (\underline{E}_t(\underline{r}) + \underline{n} \times \underline{M})/2 \\ \widehat{\underline{H}}_t(\underline{r}^-) &= +\mathcal{T}\underline{M} + \mathcal{K}\underline{J} + \underline{n} \times \underline{J}/2 = (\underline{H}_t(\underline{r}) + \underline{n} \times \underline{J})/2 \end{aligned} \tag{C5}$$

that, from Eqs. (21) and (31), yield

$$\begin{aligned} \widehat{\underline{E}}_t(\underline{r}^-) &= \frac{L_J \underline{J} - (b_1 L_D - b_2 L_R)\underline{E}_t + \underline{n} \times \underline{M}}{2} \\ \widehat{\underline{H}}_t(\underline{r}^-) &= \frac{\underline{n} \times \{L_J \underline{J} - (b_1 L_D - b_2 L_R)\underline{E}_t\} - \underline{M}}{2a_0} \end{aligned} \tag{C6}$$

that entails

$$\widehat{\underline{E}}_t(\underline{r}^-) = -a_0 \underline{n} \times \widehat{\underline{H}}(\underline{r}^-) \tag{C7}$$

Now, because $\widehat{\underline{E}}$ and $\widehat{\underline{H}}$ satisfy the source free Maxwell's equations in the free-space domain V^- inside Γ and because of Eq. (C7),

$$\begin{aligned} \int_{V^-} \left(\left| \underline{\nabla} \times \widehat{\underline{E}} \right|^2 - k^2 \left| \widehat{\underline{E}} \right|^2 \right) &= -ik \int_\Gamma \widehat{\underline{E}} \cdot \left(\underline{n} \times \widehat{\underline{H}}^* \right) \\ &= ika_0 \int_\Gamma \left| \underline{n} \times \widehat{\underline{H}} \right|^2 \end{aligned}$$

that implies $\widehat{\underline{E}}_t(\underline{r}^-) = \widehat{\underline{H}}_t(\underline{r}^-) = 0$ if $Re(a_0) \neq 0$ and, because of Eqs. (C3) and (C4),

$$\widehat{\underline{E}}_t\left(\underline{r}^+\right) = -\underline{n} \times \underline{M}; \quad \widehat{\underline{H}}_t\left(\underline{r}^+\right) = -\underline{n} \times \underline{J} \tag{C8}$$

Finally, since $\widehat{\underline{E}}$ and $\widehat{\underline{H}}$ satisfy the source free Maxwell's equations in domain V^+ outside of Γ, the IBC3 on Γ and the Silver-Müller radiation condition, we get $\widehat{\underline{E}}(\underline{r}) = \widehat{\underline{H}}(\underline{r}) = 0 \ \forall \underline{r} \in V^+$ if the SUCs are satisfied, and Eq. (C8) implies $\underline{J} = \underline{M} = 0$.

REFERENCES

1. Leontovich, M., *Investigation on Radiowave Propagation*, Part II, Academy of Sciences, Moscow, 1948.
2. Duruflé, M., H. Haddar, and P. Joly, "Higher order generalized impedance boundary conditions in electromagnetic scattering problems," *C. R. Physique*, Vol. 7, 533–542, 2006.
3. Duruflé, M., V. Péron, and C. Poignard, "Thin layer models for electromagnetism," *Commun. Comput. Phys.*, Vol. 16, No. 1, 213–238, 2014.
4. Péron, V., K. Schmidt, and M. Duruflé, "Equivalent transmission conditions for the time-harmonic Maxwell equations in 3D for a medium with a highly conductive thin sheet," *SIAM J. Appl. Math.*, Vol. 76, No. 3, 1031–1052, 2016.
5. Karp, S. N. and F. C. Karal, Jr., "Generalized impedance boundary conditions with applications to surface wave structures," *Electromagnetic Wave Theory*, Part 1, J. Brown ed., Pergamon, N. Y., 479–483, 1967.
6. Senior, T. B. A. and J. L. Volakis, *Approximate Boundary Conditions in Electromagnetics*, IEE Electromagnetic Waves Series 41, London, 1995.
7. Hoppe, D. J. and Y. Rahmat-Samii, *Impedance Boundary Conditions in Electromagnetics*, Taylor & Francis ed., 1995.
8. Marceaux, O. and B. Stupfel, "High-order impedance boundary conditions for multilayer coated 3D objects," *IEEE Trans. Antennas Propagat.*, Vol. 48, 429–436, 2000.
9. Stupfel, B. and D. Poget, "Sufficient uniqueness conditions for the solution of the time harmonic Maxwell's equations associated with surface impedance boundary conditions," *J. Comp. Phys.*, Vol. 230, 4571–4587, 2011.

10. Stupfel, B., "One-way domain decomposition method with adaptive absorbing boundary condition for the solution of Maxwell's equations," *IEEE Trans. Antennas Propagat.*, Vol. 61, No. 10, 5100–5108, 2013.
11. Stupfel, B., "Implementation of high order impedance boundary conditions in some integral equation formulations," *IEEE Trans. Antennas Propagat.*, Vol. 63, No. 4, 1658–1668, 2015.
12. Aubakirov, A., "Electromagnetic scattering problem with higher order impedance boundary conditions and integral methods," Ph.D. dissertation, Université de Cergy-Pontoise, France, 2014.
13. Soudais, P., "3D MoM computations with high order impedance boundary conditions in some integral equation formulations," *Int. Conf. in Electromagnetics and Applications*, Verona, September 2017.
14. Bendali, A., M'B. Fares, and J. Gay, "A boundary element solution of the Leontovich problem," *IEEE Trans. Antennas Propagat.*, Vol. 47, No. 10, 1597–1605, 1999.
15. Yan, S. and J. M. Jin, "Self-dual integral equations for electromagnetic scattering from IBC objects," *IEEE Trans. Antennas Propagat.*, Vol. 61, No. 11, 5533–5546, 2013.
16. Li, W. D., W. Hong, H. X. Zhou, and Z. Song, "Novel Buffa-Christianssen function for improving CFIE with impedance boundary conditions," *IEEE Trans. Antennas Propagat.*, Vol. 60, No. 8, 3763–3771, 2012.
17. Stupfel, B. and M. Chanaud, "High-order transmission conditions in a domain decomposition method for the time-harmonic Maxwell's equations in inhomogeneous media," *J. Comp. Phys.*, Vol. 372, 385–405, 2018.
18. Kong, J. A., *Electromagnetic Wave Theory*, John Wiley & Sons, 1986.
19. Stupfel, B., "Homogenization of a multilayer coating. Application to model-order reduction," *IEEE Trans. Antennas Propagat.*, Vol. 69, No. 3, 1528–1534, 2021.
20. Stupfel, B. and M. Mognot, "Implementation and derivation of conformal absorbing boundary conditions for the vector wave equation," *J. Electromag. Waves and Appl.*, Vol. 12, No. 12, 1653–1677, 1998.
21. Nédélec, J. C., *Acoustic and Electromagnetic Equations — Integral Representations for Harmonic Problems*, Springer-Verlag, 2001.
22. Stupfel, B., "Characterization of surface waves in a multilayer coating. Application to far-field control," *IEEE Trans. Antennas Propagat.*, Vol. 69, No. 6, 3623–3627, 2021.
23. Stupfel, B., R. Le Martret, P. Bonnemason, and B. Scheurer, "Combined boundary-element and finite-element method for the scattering problem by axisymmetrical penetrable objects," *Proceedings of the International Symposium on Mathematical and Numerical Aspects of Wave Propagation Phenomena*, 332–341, SIAM ed., 1991.
24. Van Bladel, J. G., *Electromagnetic Fields*, 2007.
25. Howell, W. E. and H. Uberall, "Selective observation of resonances via their ringing in transient radar scattering, as illustrated for conducting and coated spheres," *IEEE Trans. Antennas Propagat.*, Vol. 38, 1990.
26. Taylor, D. J., A. K. Jordan, P. J. Moser, and H. Uberall, "Complex resonances of conducting spheres with lossy coatings," *IEEE Trans. Antennas Propagat.*, Vol. 38, No. 2, 236–240, 1990.
27. Stupfel, B. and Y. Pion, "Impedance boundary conditions for finite planar and curved frequency selective surfaces," *IEEE Trans. Antennas Propagat.*, Vol. 53, No. 4, 1415–1425, 2005.
28. Stupfel, B., "Impedance boundary conditions for finite planar and curved frequency selective surfaces embedded in dielectric layers," *IEEE Trans. Antennas Propagat.*, Vol. 53, No. 11, 3654–3663, 2005.